J Therm Spray Tech (2021) 30:2099–2116
https://doi.org/10.1007/s11666-021-01269-w

PEER REVIEWED

Development of Cold Sprayed Titanium/Baghdadite Composite Coating for Bio-implant Applications

Avneesh Kumar[1] · Harpreet Singh[1] · Ravi Kant[1] · Nahida Rasool[1]

Submitted: 1 June 2021 / in revised form: 25 August 2021 / Accepted: 11 October 2021 / Published online: 5 November 2021

Abstract Titanium/Baghdadite composite coatings have been deposited on SS316L using cold spray technology to explore their potential use as bio-implant coatings. Microstructural and mechanical characterization have been conducted to evaluate the quality of the coatings. The electrochemical corrosion behavior of the developed coatings has been evaluated in a simulated body fluid environment. The results show that baghdadite content influenced the corrosion resistance of coatings; more the baghdadite content, better is the corrosion resistance. In general, the developed coatings were successful in enhancing the corrosion resistance of SS316L. Also, the developed coatings outperformed earlier reported cold sprayed titanium/hydroxyapatite composite coatings.

Keywords baghdadite · bio-implant coating · cold spray · electrochemical impedance spectroscopy · polarization

Introduction

Arthritis is a common cause of hip joint failures. Intra-articular steroid injections (IASI) therapy and implantation are the two major solutions for recovering normal functioning of the hip joint. IASI has several drawbacks, including short life expectancy (few months), chances of infection during injection, and painful treatment (Ref 1). Therefore, hip arthroplasty which has a longer life of 10-15 years is generally advised (Ref 2). The useful life of hip implants in the human body environment is restricted owing to several degradations occurring in the human body environment, including corrosion and wear. Such degradation may be controlled either by using highly expensive standalone bio-corrosion or wear-resistant materials or by surface modification of the existing economic biomaterials.

Corrosion is defined as the deterioration of material while exposed to the surrounding environment. It is one of the major reasons behind the failure of metals and their alloys when implanted in the human body (Ref 3). The human body environment is highly corrosive; implants release ions in the human body through chemical or electrochemical reactions. These chemical reactions proceed toward a thermodynamic equilibrium, which can be evaluated through electrochemical behavior testings in electrochemical cells. In electrochemical cells, oxidation and reduction are the two important processes taking place at the anodic and cathodic sites, respectively. At an anode, metal or its alloys are forced to release electrons by supplying electric energy from the external source, which leads to oxidation at the anode. At equilibrium, electrons flowing on both the surfaces become equal, and hence, the net current flow into the cell becomes zero. In other words, the rate of oxidation and reduction becomes equal. At equilibrium, the current flowing through the electrodes is called corrosion current (I_{corr}), and the respective corresponding voltage is called open circuit potential or corrosion potential (E_{ocp} or E_{corr}) (Ref 4).

Since the development of Arthroplasty, the use of material became critically important. Several materials are proposed for the intended application, such as ivory, stainless steel, cobalt-chromium alloys, and titanium and their alloys (Ref 5-8). Titanium and its alloys are popular for their superior corrosion resistance in the human body

✉ Harpreet Singh
harpreetsingh@iitrpr.ac.in

[1] Department of Mechanical Engineering, Indian Institute of Technology Ropar, Punjab 140001, India

environment (Ref 9) due to the rapid formation of the passive surface film of titanium oxide, which helps in reducing the ion release (Ref 10, 11). However, these alloys, due to their higher cost and lack of osseointegration, are not suitable for implant applications. Calcium phosphate compounds such as hydroxyapatite (HA) help in improving bioactivity and osseointegration between the implant and the bone (Ref 12, 13). Therefore, in order to take advantage of both Ti and HA, Ti/HA composite materials are developed (Ref 14). Anawati et al. (Ref 15) reported that the bioactivity and corrosion behavior of Ti-HA composite are better compared to the standalone titanium. Although HA is well accepted biomaterial, however, it lacks in terms of mechanical properties. As an alternative to HA, baghdadite (BAG– $Ca_3ZrSi_2O_9$) is a calcium silicate compound that exhibits excellent biological (Ref 16, 17) properties along with better mechanical characteristics as compared to HA (Ref 18-22). Coating of these materials on a cheaper base material may give an economically viable solution with enhanced overall performance of the implants. In this context, acceptable mechanical properties and low price of SS316L steel make it one of the most widely used first-generation bio-implants such as hip and knee implant (Ref 6, 23).

Thermal spray techniques are the most widely accepted surface modification techniques for depositing above-mentioned materials over the substrate. However, high temperature is involved in the thermal spray processing, which may pose several defects in the coating, such as a phase change and oxidation (Ref 24). On the other hand, cold spray is a low-temperature solid-state coating deposition technique which has many advantages over thermal spray techniques. Temperature-sensitive materials like titanium and its alloys can be sprayed without any change in powder characteristics (Ref 25). The feedstock powder particles are propelled by supersonic gas and deposited on the substrate. The cold sprayed coatings are less porous and possess better corrosion resistance (Ref 26).

In view of the above discussion, a maiden effort has been made to develop Ti/BAG-based composite coating on SS316L steel by cold spray technique. Subsequently, the coatings' electrochemical corrosion behavior has been evaluated in Ringer's solution to explore the potential of the developed coatings for biomedical applications. Potentiodynamic polarization and electrochemical impedance spectroscopy (EIS) corrosion analyses were performed on four different compositions of Ti/BAG. The results indicate that the presence of BAG content in the coating helped in improving the corrosion resistance of the coatings.

Experimental Procedure

Materials and Deposition of Coatings

Commercially available SS316L steel was selected as the substrate material for the current study as it is frequently used for manufacturing economical bio-implants. Chemical composition of the steel is reported in Table 1. Ti (Nanoresearch Elements, US) and BAG powders with 99% purity were used as the feedstock materials to develop Ti/BAG-based composite coatings. BAG is fabricated by mixing zirconium oxide (ZrO_2), silica (SiO_2), and calcium carbonate ($CaCO_3$) powders in a molar ratio of 1:2:3, followed by sintering. The obtained mixture was crushed to get the given BAG powder (Ref 18). Ti powder was prepared using pyrometallurgical process. Figure 1 depicts the morphology of Cp-Ti and BAG powders. Phase analysis of the powders (Fig. 2) was also performed to check their purity. Ti and BAG powders were mixed in various (wt.%) ratios to develop four composite compositions, as shown in Table 2. The mixing was done using a magnetic stirrer (Optima, MS 300) operating at 1000 rpm for 30 min at room temperature. Steel substrates were mirror polished before deposition of the coatings using emery papers down to 2000 grit and then ultrasonically cleaned with acetone with an aim to achieve good adhesion with the coatings. Subsequently, the Ti/BAG powders were deposited on the steel substrate by a cold spray gun (Plasma Giken, PCS-101, Japan) having a convergent-divergent, (De-laval) nozzle with a circular cross section. All the coatings were prepared using nitrogen as the process gas at a uniform pressure of 30 bar and temperature of 900 °C.

Microstructural and Mechanical Characterization

The cross-sectional analysis of the cold sprayed Ti/BAG composite coatings was performed using scanning electron microscopy, SEM (JEOL, JSM-6610 LV, Japan), and energy-dispersive spectroscopy, EDS (JEOL, JSM-6610 LV, Japan). The samples were sectioned using a wire-cut electric discharge machine (EDM, ELECTRONICA, SPRINTCUT, India), following a standard guide for metallographic preparation of thermally sprayed coatings (ASTM E-1920) (Ref 27). To avoid any effects of temperature, the specimens were cold-mounted and then polished down to 2000 grit using emery papers**.** The phase identification in the developed coatings was performed by x-ray diffraction, XRD (Analytical X-pert Pro, Netherland) using Cu-Kα radiation. XRD data was taken in the 2θ range of 10-90° with a scanning speed of 1 kcps. The surface roughness of the developed coatings was measured using a roughness tester (HandySurf E-35-A/B, Accretech, Japan)

Table 1 Chemical composition of SS316L steel substrate used for the cold spray Ti/BAG coatings

Elements	Fe	Cr	Ni	Mo	Mn	C	P	Si
Composition, %	Balance	16.17%	10.02%	2.06%	0.87%	0.018%	0.03%	0.23%

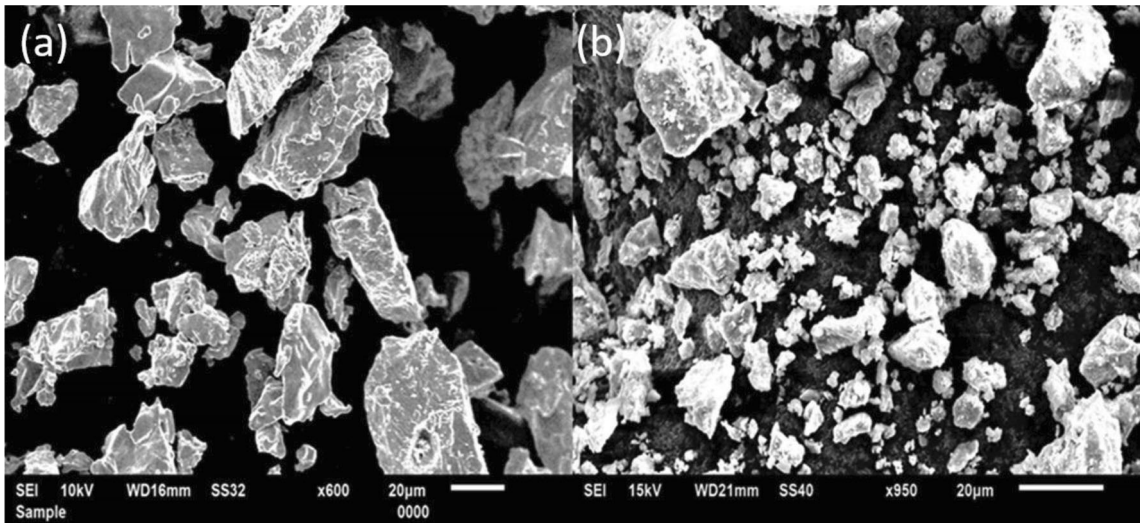

Fig. 1 SEM micrographs of feedstock powders (a) Titanium (b) BAG used for the development of cold sprayed Ti/BAG composite coating

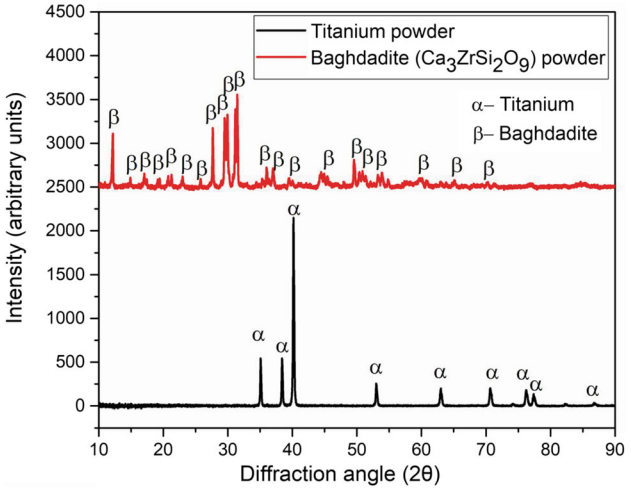

Fig. 2 XRD analysis of the feedstock powders used for the development of cold spray Ti/BAG composite coatings on SS316L

in terms of arithmetic mean deviation (Ra). Roughness measurements were performed with the cutoff length of 2 mm and a measuring speed of 0.5 mm/second. Ten values of the roughness parameter were taken for each coating, and subsequently, the average of these values is reported for each case. The porosity of the samples was calculated following ASTM B962-15 (Ref 27). The following equation is used to calculate the porosity of the coatings (Ref 28):

Table 2 Details of the cold sprayed Ti/BAG-based composite coatings investigated in the present study

S. No.	Coating designation	Composition (wt.%)	
		Ti	BAG
1	Ti/10BAG	90	10
2	Ti/15BAG	85	15
3	Ti/20BAG	80	20
4	Ti/25BAG	75	25

$$\%\text{porosity} = \left(\frac{V_w - V_a}{V_a}\right) \times 100, \qquad \text{(Eq 1)}$$

where V_w and V_a are the volume of the coating after curing into the water for 24 h and the volume of the coating after dried into the vacuum of 250 mbar at room temperature for 24 h, respectively. Mass of the coating samples was measured by curing it in the water and again after drying in the vacuum using a mass balance with an accuracy of 0.001 g. The density of all the coating compositions was measured using a density meter (METTLER TOLEDO, MS 105, Switzerland) with an accuracy of 0.01 mg. Based on the measured values of the mass and density, the volume was calculated.

Table 3 Input parameters for potentiodynamic scan and EIS analysis of uncoated and cold sprayed Ti/BAG coated SS316L specimens

Parameters	Value
Initial potential	− 250 mV versus open circuit potential
Final potential	250 mV versus open circuit potential
Scan rate	1 mV/s
Exposed sample area	1 cm^2
Frequency range	1000 kHz to 100 MHz
Initial delay	3600 s

Electrochemical Corrosion Analysis

Potentiodynamic polarization and electrochemical impedance spectroscopy (EIS) were performed to check the efficacy of the cold sprayed Ti/BAG composite coatings on SS316L against corrosion. The medium for corrosion testing was Ringer's solution having a chemical composition of 9 g/L of NaCl, 0.24 g/L of $CaCl_2$, 0.43 g/L of KCl, and 0.2 g/L of $NaHCO_3$. The samples were tested in a standard 3-electrode electrochemical cell (PTC1, Gamry Instruments, US) at room temperature. The specimens were used as working electrodes, Ag/AgCl as a reference electrode and graphite as the counter electrode. The input parameters used for the testings are given in Table 3. Tafel extrapolation method was used to determine the corrosion potential and corrosion current from the polarization curves of coated and uncoated samples. Echem analysis software was used for the analysis of the data.

Biocompatibility Analysis

The cell viability of the developed coatings was performed on mouse preosteoblast cells (MC3T3-E1, passage 11-12) using reported protocol with slight modification (Ref 29). The cells were cultured in tissue culture treated 25 flask with media MEM-α, containing 10% fetal bovine serum (FBS, Gibco) with 1% antibiotic solution. The culture medium was replenished every 48 h, and the sub-confluent cells were harvested using the trypsin-EDTA solution. Approximately 10,000 cells/well were seeded in treated tissue culture using 48 well plates and incubated for 24 h in a humidified atmosphere having 5% CO_2 at 37 °C. The samples were suspended in ethanol, sonicated for 30 min, and air-dried. The sterilization was done using a UV light for 30 min. Each sample was incubated in α-MEM media for 24 h at 37 °C and then passed through a 0.22 µm syringe filter. The media of cells cultured in 48 well plates were replaced with filtered extracts, and cells were further incubated for 24 h. An amount of 30 µL MTT solution (5 mg/mL) was added to each well, and the plate was incubated at 37 °C for 3.5 h. The resulting formazan crystals were dissolved in DMSO (100 µL), and absorbance was recorded at 570 nm using a Tecan Infinite M Plex plate reader. The percentage of cell viability was calculated by comparing the absorbance of treated cells with the untreated cells.

Results and Discussion

Characterization of Coatings

The powders are irregular in shape (Fig. 1), which is a desirable attribute since such particles need lesser energy to attain critical velocity for the deposition in cold spray (Ref 30-32). There are lot of contradictions about the surface preparation in cold spray. Some recent studies revealed that mirror polished surfaces promote better adhesion. For instance, Tanvir et al. (Ref 33) have shown that mirror polished aluminum alloy substrate surface led to a better bonding of copper particles. Similarly, Singh et al. (Ref 34) experimentally proved in their work that mirror polished steel surfaces are good for adhesion between the copper coating and steel substrate. A sufficient plastic deformation and better jetting formation of copper particle on mirror polished steel substrate during the deposition were ascribed the reasons for better adhesion in cold spray (Ref 34). The cross-sectional micrographs of the as-sprayed Ti/BAG composite coatings are shown in Fig. 3. From the micrographs, it is clear that the coatings are in continuous contact with the respective mirror polished steel substrate, and there are no void or cracks at the interfaces. Ti particles are completely deformed and integrated into the layers. However, there is a presence of micro-pores along some of the particle–particle interfaces. The number of pores increases with the increase in the BAG content. The void formation may be attributed to the ceramic nature of BAG, which on solid-state impact (cold spray) would result in fracture of the particle (Ref 35). Figure 4 shows the XRD analysis of the cold sprayed Ti/BAG composite coatings. The results indicate no change in phase post-cold spraying, which is a desirable feature for our application. Also, post-spraying titanium peaks were observed a little wider compared to powder peaks in XRD data. It is because of the plastic deformation of the powder particles while spraying. Figure 5 shows the elemental mappings of the cold sprayed Ti/BAG composite coatings along their cross sections and top surfaces, respectively. The mappings reveal that in Ti/BAG composite coatings, the major elements present are titanium (Ti), calcium (Ca), silicon (Si), oxygen (O), and zirconium (Zr). The mappings also show that Ti and BAG

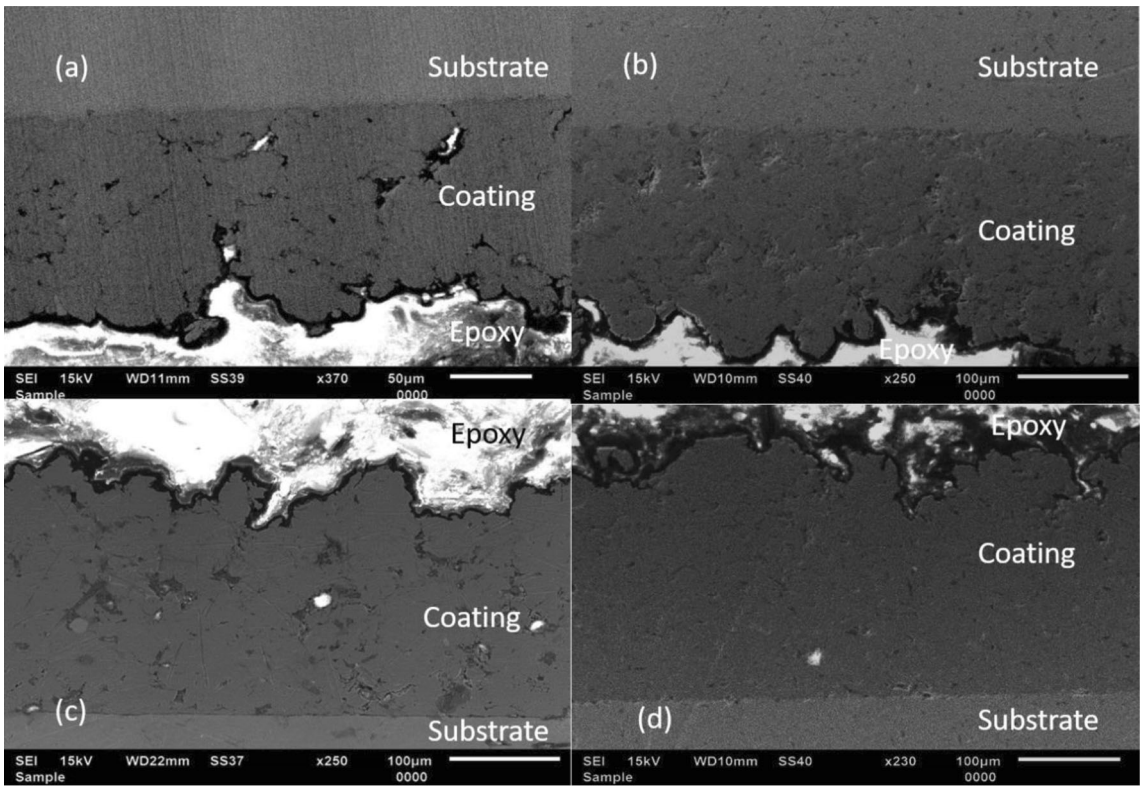

Fig. 3 Cross-sectional SEM micrographs of cold sprayed Ti/BAG composite as-sprayed coatings on SS316L steel substrate (a) Ti/25 BAG (b) Ti/20 BAG (c) Ti/15 BAG (d) Ti/10 BAG

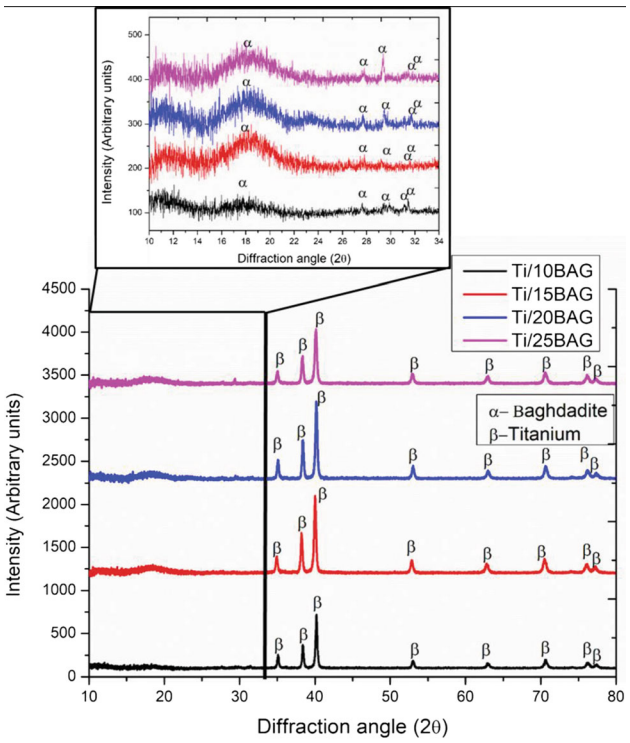

Fig. 4 XRD analysis of cold sprayed Ti/BAG composite coatings on SS316L

constituents prevail at alternate locations in the coating microstructure, indicating a typical metal matrix (Ti) composite embedded with the secondary phase (BAG). The Image J software was used to analyze and calculate volumetric retention from cross-sectional SEM/EDS images (Fig. 5). Further, volumetric retention was converted into weight retention. These analysis indicate that BAG content has reduced after the deposition in the range of 20-35% depending upon the coating composition. Moreover, the distribution of BAG in the coatings is found to be non-homogeneous. Surface SEM images along with chemical compositions are also reported, as shown in Fig. 6. The results revealed that the BAG was successfully deposited in the Ti matrix using the cold spray, and good quality of coatings is achieved.

From Fig. 3 and ImageJ software (ten readings per each coating), it is clear that the coating thickness (Fig. 7a) is decreased continuously from 236 ± 11 µm to 153 ± 8 µm with the increment in BAG content which may be because of the increment in ceramic content. It is reported that the increase in ceramic content reduces the bonding strength between the particles (Ref 36). It is pertinent to mention that the number of passes was kept the same in all the cases. The interaction between BAG-BAG particles dominates with the increment in BAG content. Since it is well

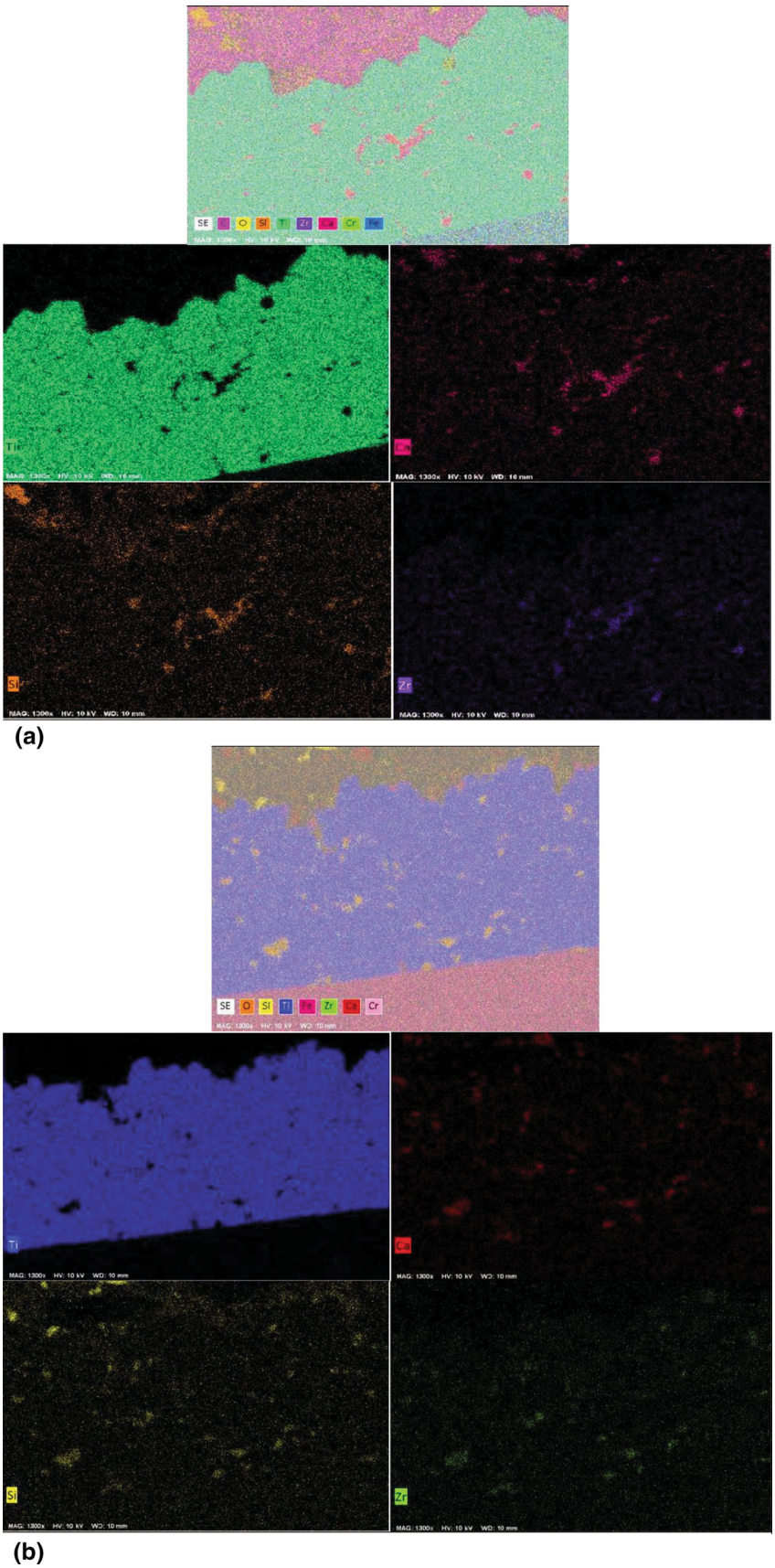

Fig. 5 (a) Cross-sectional EDS mappings of the cold sprayed Ti/10BAG composite coatings on SS316L. (b) Cross-sectional EDS mappings of the cold sprayed Ti/15BAG composite coatings on SS316L. (c) Cross-sectional EDS mappings of the cold sprayed Ti/20BAG composite coatings on SS316L. (d) Cross-sectional EDS mappings of the cold sprayed Ti/25BAG composite coatings on SS316L

Fig. 5 continued

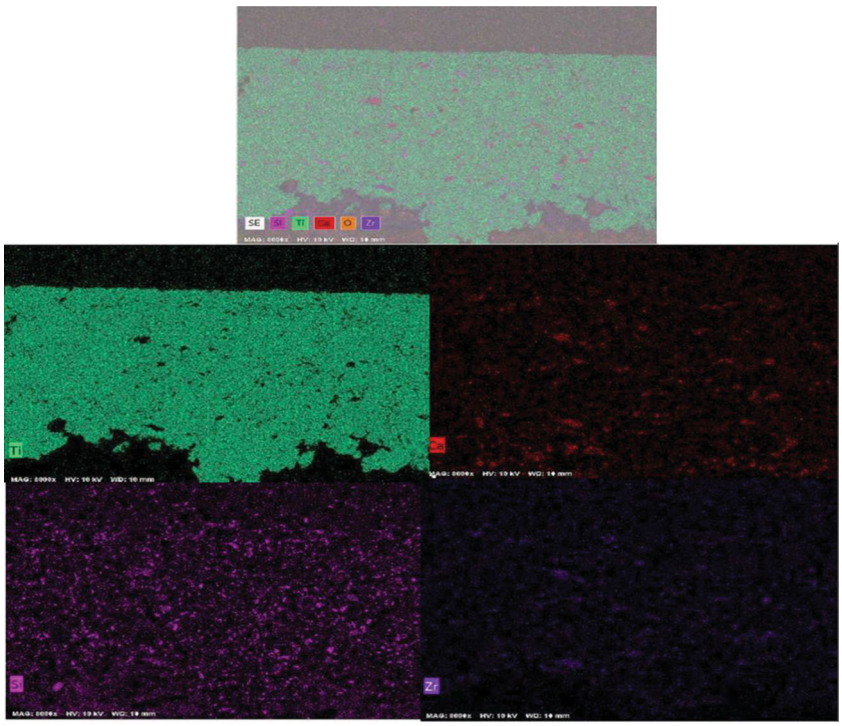

(c)

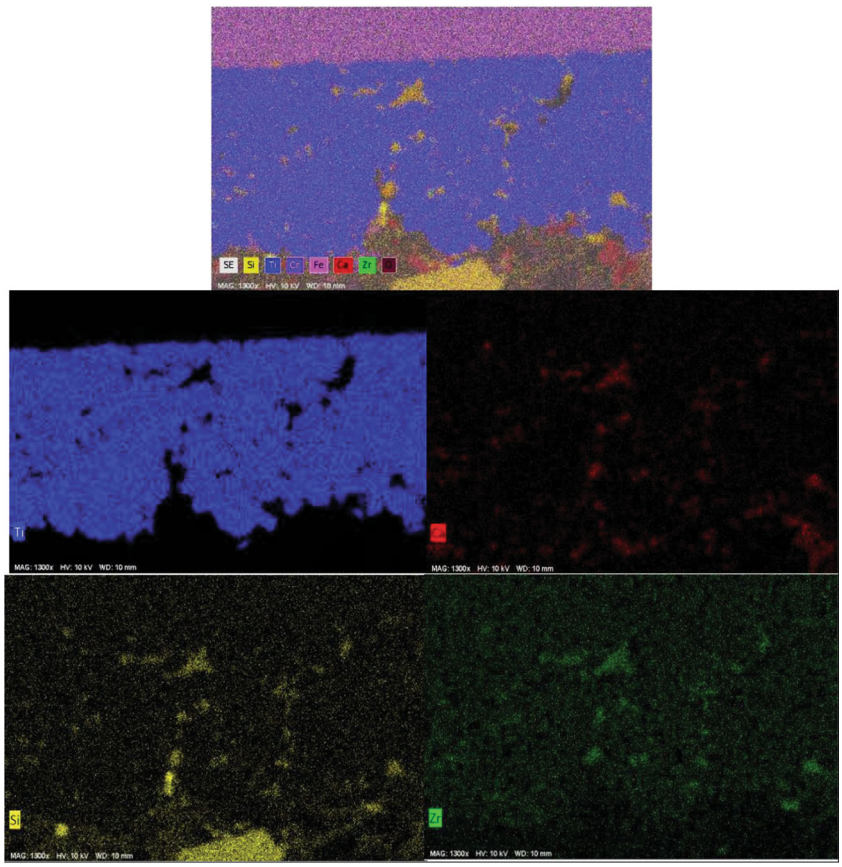

(d)

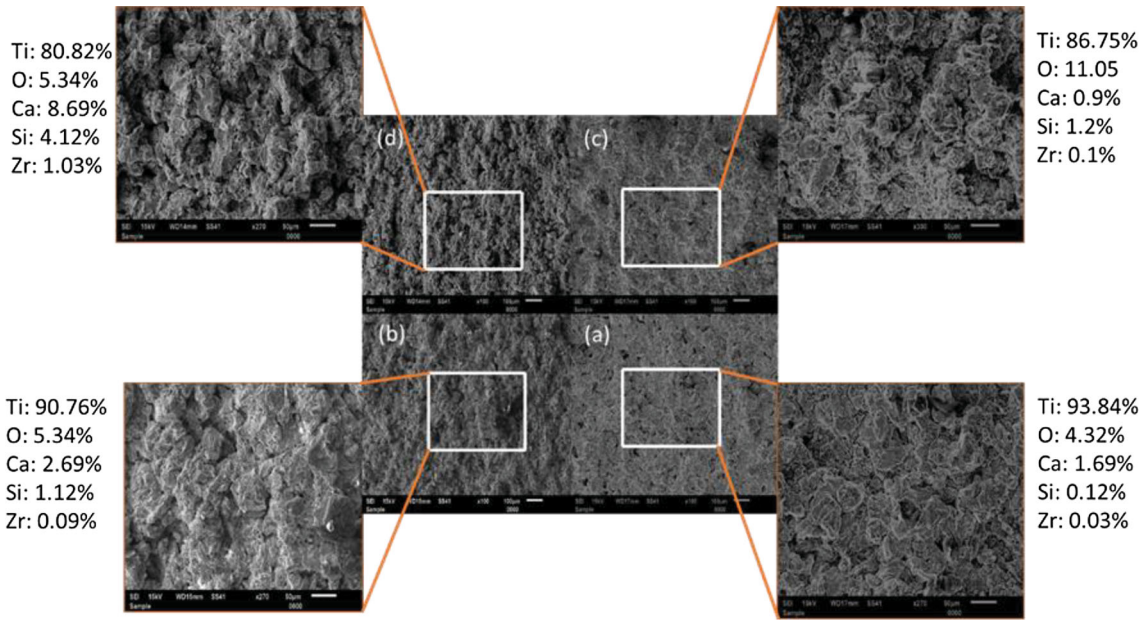

Fig. 6 Surface SEM micrographs of the cold sprayed Ti/BAG composite coatings on SS316L substrate with chemical compositions (a) Ti/10BAG (b) Ti/15BAG (c) Ti/20BAG (d) Ti/25BAG

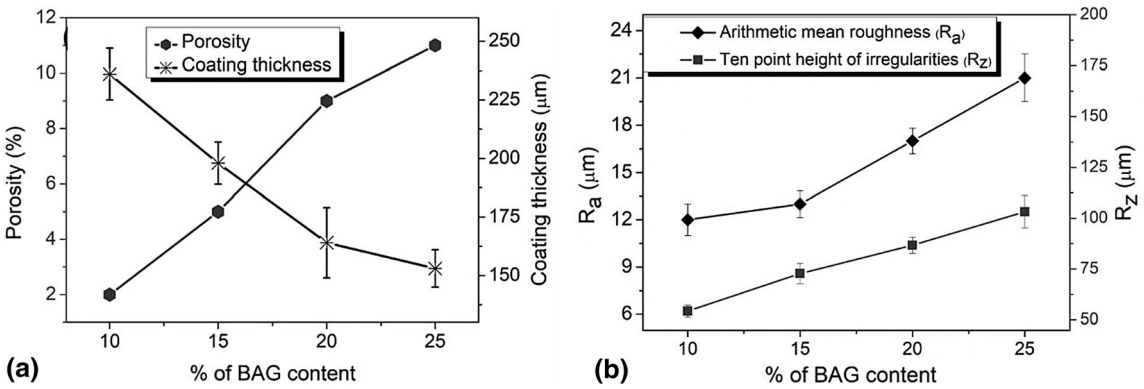

Fig. 7 (a) Porosity and coating thickness (b) surface roughness analysis of the as-received cold spray Ti/BAG composite coatings on SS316L

known that the ceramic particles do not bond with each other, therefore a drop in deposition efficiency is expected, leading to lesser coating thickness with the same number of passes as the BAG content is increased. Similar results were reported by Wang et al. (Ref 37) and Irissou et al. (Ref 38). Sousa et al. (Ref 39) reported that coatings around 200 μm thick are sufficient to develop a barrier to corrosion. Being a new material and substrate combination, several trial experiments were conducted (Gas pressure range: 15-30 bar and gas temperature range: 600-900 °C) to arrive at the reported parameters. The coating thickness was chosen as the output response with 200 μm as the threshold value. From the results shown in Fig. 7(a), it is observed that the porosity of the sample increases with the increment of BAG content. It may be because when ceramic/metallic particles impact on metallic/ceramic particles, ceramic particles either fracture or show no significant plastic deformation and lead to poor bonding or voids/gaps at the splat boundaries (Ref 40, 41). As the ceramic content increases, this interaction of ceramic–ceramic particles or ceramic–metallic particles also increases, leading to more voids/gaps at the splat boundaries. Porosity may or may not affect the coating's corrosion performance, but it affects the osseointegration (Ref 42). Surface roughness plays a vital role in biomedical coatings as it provides more surface area for cell adhesion or cell growth. Simultaneously, surface roughness also affects the corrosion performance as it allows more area to corrode (Ref 43). The results plotted in Fig. 7(b) indicate the improvement in as-sprayed surface roughness with BAG content progression. From the graph, it can be observed that an increase in surface roughness from Ti/10BAG to Ti/15BAG is way less than Ti/15BAG

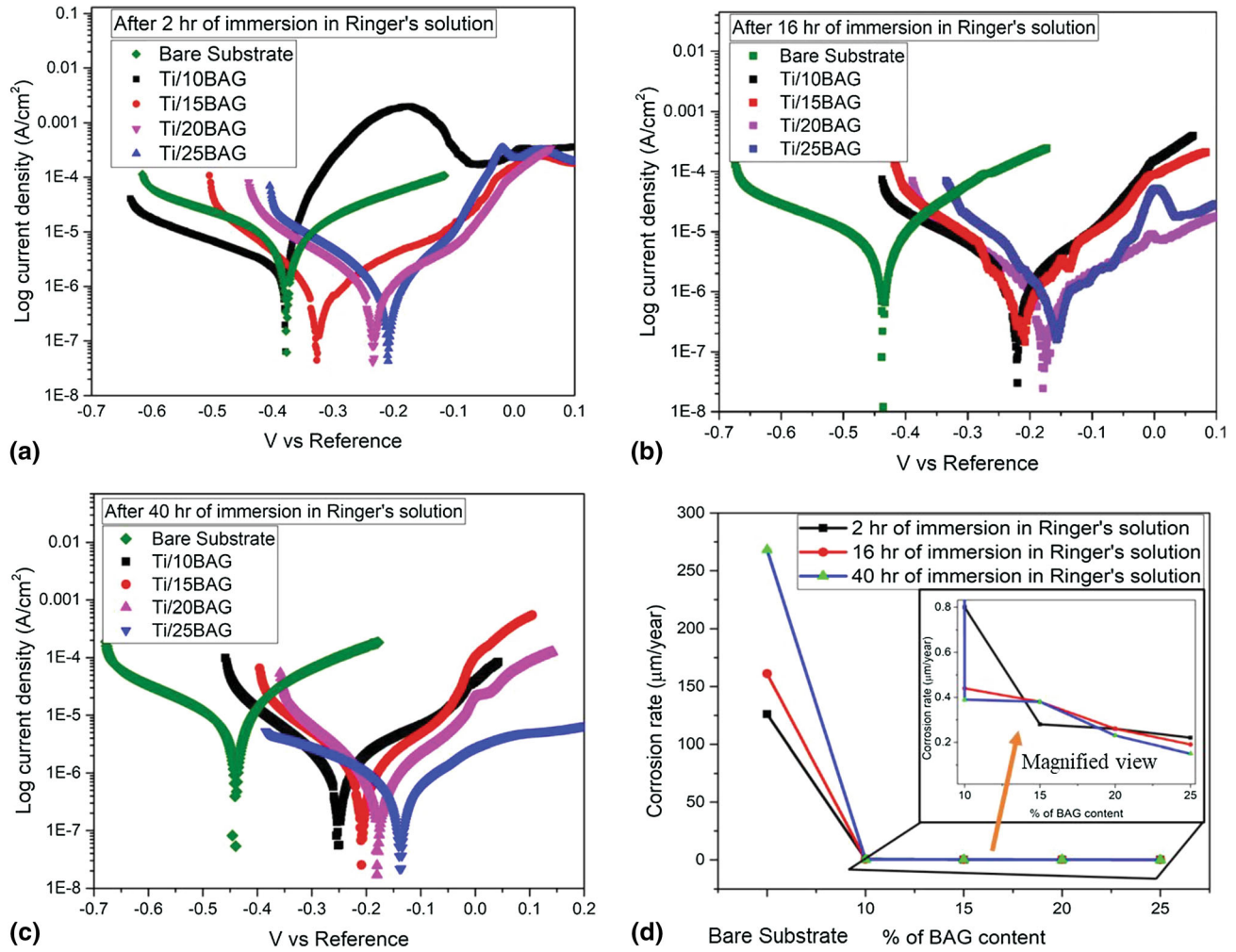

Fig. 8 Potentiodynamic polarization behavior of bare and cold spray Ti/BAG coated SS316L in Ringer's solution (a) after 2 h of immersion (b) after 16 h of immersion (c) after 40 h of immersion, and (d) the corrosion rate

to Ti/20BAG and Ti/20BAG to Ti/25BAG coatings. It may be due to the fact that with an increase in ceramic content, chances to get bonded with the metallic particles on the top layer will decrease due to the increase in the interaction of ceramic–ceramic particles. As ceramic content increases, deposition efficiency decreases due to the increment in ceramic–ceramic particle interaction. In other words, more particles rebound without bonding and lead to relatively higher tamping effect (Ref 44, 45). However, irregular powders morphology was observed to leave a very less tamping effect and results in higher porosity and greater roughness (Ref 46, 47).

Electrochemical Corrosion Performance

The electrochemical reactions between the coating and the electrolyte lead to the degradation of the coatings. Potentiodynamic polarization curves of bare SS316L and cold sprayed Ti/BAG composite coating with different percentages of BAG and immersion time in Ringer's solution are shown in Fig. 8(a), (b), and (c). The open circuit potential of the steel is found to be the lowest in a simulated body fluid environment. The results indicate a notable improvement in thermodynamic stability of SS316L after the deposition of the cold sprayed coatings in simulated body fluid. The open circuit potential of the developed coatings is shifted in the noble direction with the increase in BAG content and immersion time. It is because Ti forms a passive layer of titanium oxide when exposed to Ringer's solution. Also, the presence of BAG in the cold sprayed Ti/BAG composite coating helps to release calcium, silicon, and zirconium ions, which form oxides of Ca, Si, and Zr, respectively. The results (Table 4) depict that the corrosion current has also decreased as the composite layer of Ti and BAG serves as a barrier to corrosion between the simulated body fluid and the substrate. In other words, the coatings have lowered the release of ions and electrons. The corrosion rate of composite coatings has also

Table 4 Corrosion parameters of cold sprayed Ti/BAG composite coatings on SS316L in Ringer's solution

S. No.	Sample ID	E_{corr}, mV	Log I_{corr}, μA/cm^2	β_α, mV	β_c, mV	Corrosion rate, μm/year
(a) After 2 h of immersion in Ringer's solution						
1	Substrate	− 377.5	3.24	9.02 ± 0.4	− 8.032 ± 0.12	126.4
2	Ti/10BAG Coating	− 381.38	2.29	36.35 ± 0.88	− 4.05 ± 0.02	0.806
3	Ti/15BAG Coating	− 326.58	0.807	4.384 ± 0.09	− 9.57 ± 0.0.05	0.284
4	Ti/20BAG Coating	− 233.34	0.748	6.80 ± 0.07	− 8.89 ± 0.06	0.263
5	Ti/25BAG Coating	− 208.52	0.627	9.66 ± 0.155	− 10.97 ± 0.11	0.221
(b) After 16 h of immersion in Ringer's solution						
1	Substrate	− 435.23	3.83	8.31 ± 0.05	− 6.04 ± 0.03	161.5
2	Ti/10BAG Coating	− 218.13	1.258	8.05 ± 0.065	− 9.429 ± 0.160	0.443
3	Ti/15BAG Coating	− 209.73	1.099	8.42 ± 0.246	− 9.756 ± 0.308	0.387
4	Ti/20BAG Coating	− 176.50	0.7634	7.29 ± 0.057	− 10.367 ± 0.08	0.269
5	Ti/25BAG Coating	− 157.8	0.540	8.62 ± 0.783	− 9.693 ± 0.565	0.19
(c) After 40 h of immersion in Ringer's solution						
1	Substrate	− 441.09	6.39	10.12 ±0.002	− 9.03 ± 45	268.2
2	Ti/10BAG Coating	− 248.03	1.125	8.32 ± 0.064	− 8.497 ± 0.083	0.396
3	Ti/15BAG Coating	− 208.29	1.104	11.23 ± 0.025	− 9.114 ± 0.070	0.388
4	Ti/20BAG Coating	− 178.30	0.668	9.48 ± 0.035	− 9.048 ± 0.033	0.235
5	Ti/25BAG Coating	− 136.8	0.437	9.78 ± 0.036	− 8.113 ± 0.074	0.154

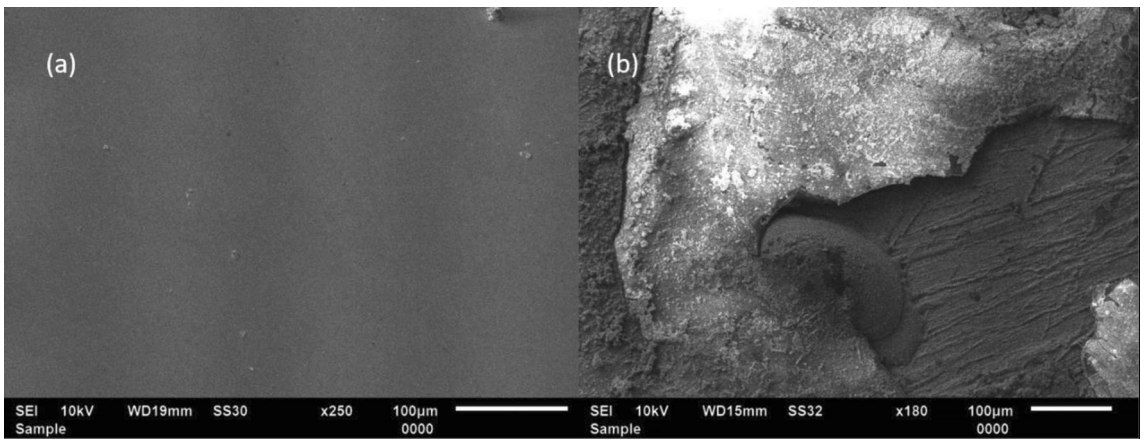

Fig. 9 Surface SEM micrographs of SS316L (a) before corrosion (b) after corrosion

been lowered compared to bare SS316L, as shown in Table 4. The potentiodynamic scans show significant improvement in corrosion performance of the coatings relative to the uncoated samples in the simulated body fluid. Stability and corrosion rate also depend on the immersion time of the coating in Ringer's solution. Figure 8(d) depicts that corrosion rate decreased with the increment in BAG content and immersion time.

SEM micrographs of the bare substrate and composite coatings after immersion in Ringer's solution are reported in Fig. 9, 10, 11 and 12. Deterioration of SS316L steel bare substrate is clearly visible. The surface layer of the SS316L has peeled off during the 40 h of exposure in Ringer's solution, as shown in Fig. 9. SEM micrographs of Ti/BAG composite coatings after 2 h, 16 h, and 40 h of immersion in Ringer's solution look better relative to bare SS316L; as no crack was observed over the surfaces. For confirming the inert, protective layer over the surface, elemental analysis using EDS was performed. The elemental analysis shown in Fig. 10, 11 and 12 indicates that the corroded coatings have more than 65% oxygen in their surface composition, whereas the oxygen content before corrosion was less than 12% for each of the coating surfaces, as shown in Fig. 7. These observations indicate the formation of a protective oxide layer over the surface. A composite coating having Ti/25BAG was mapped for the elemental

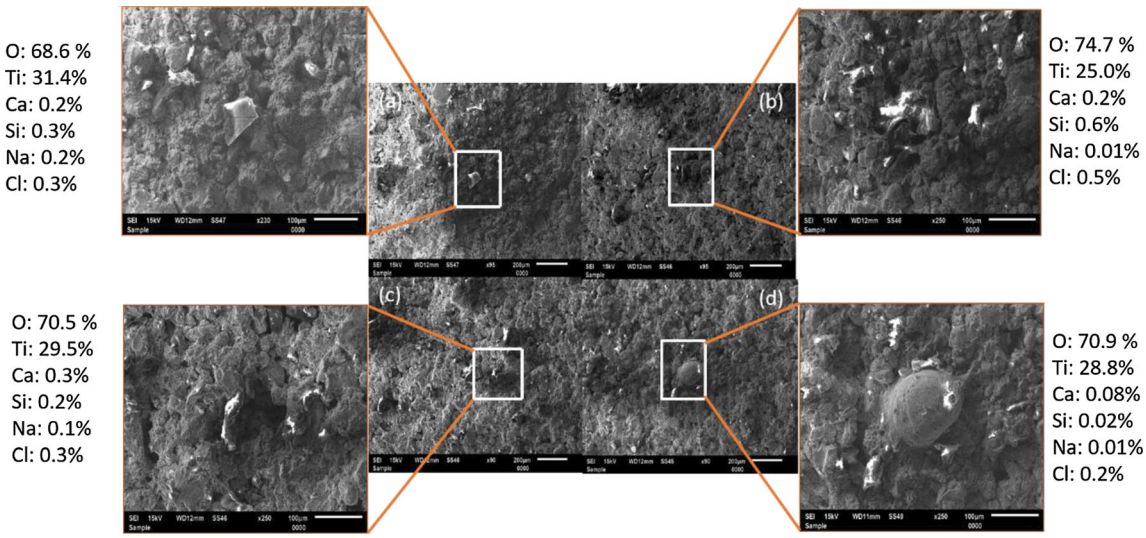

Fig. 10 Surface SEM micrograph of corroded cold sprayed Ti/BAG composite coatings after immersion in Ringer's solution for 2 h (a) Ti/10BAG (b) Ti/15BAG (c) Ti/20BAG (d) Ti/25BAG

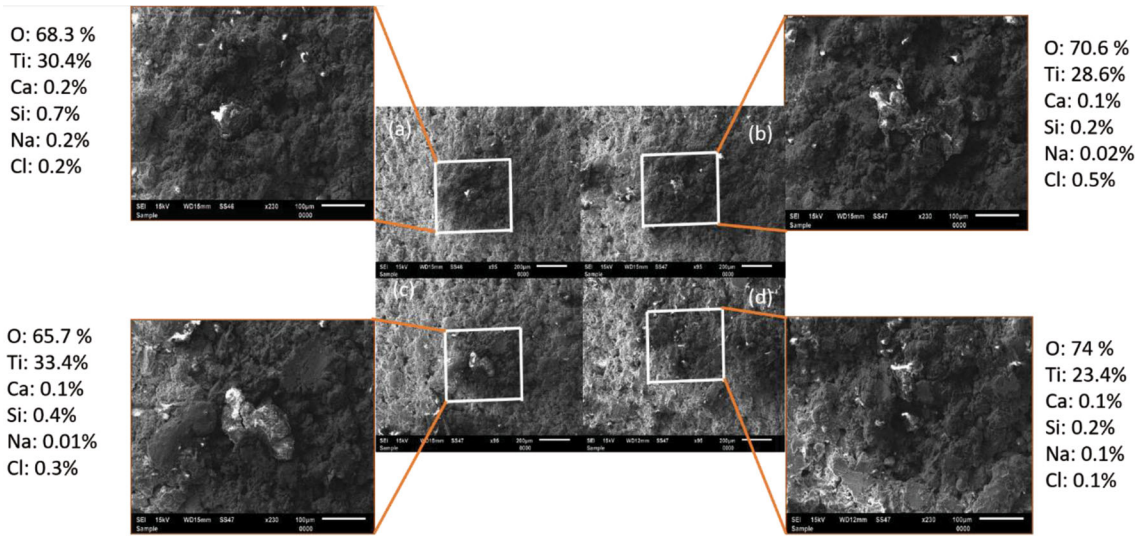

Fig. 11 Surface SEM micrograph of corroded cold sprayed Ti/BAG composite coatings after immersion in Ringer's solution for 16 h (a) Ti/10BAG (b) Ti/15BAG (c) Ti/20BAG (d) Ti/25BAG

analysis by EDS after exposing to Ringer's solution for 2 h, as shown in Fig. 13. Cross-sectional SEM/EDS analysis also supports the formation of a passive oxide layer over the surface, as shown in Fig. 14. These passivities of corrosion layers are further confirmed by XRD analysis of the exposed samples (Fig. 15). The analysis confirms the formation of TiO_2, CaO, and SiO_2 protective oxides in the exposed samples. Marino et al. (Ref 36), in their study, have also reported that Ti forms a stable and protective layer of TiO_2 in a body fluid environment. The formation of these protective oxides of Ti, Si, and Ca increases with the increase in immersion time and produces a barrier to corrosion by separating the composite from its environment (Ref 48). The thickness of the TiO_2 passive layer in titanium-based coatings usually ranges from 3-10 nm (Ref 49). SiO_2 is well known for its anti-corrosion and biological properties (Ref 50, 51). Catauro et al. (Ref 52) reported the anti-corrosion effect of ZrO_2-SiO_2 composite coatings over titanium substrate in their study. Krupa et al. (Ref 53) revealed in their studies that the implantation of calcium ions over titanium leads to the formation of CaO, which further helps in improving the corrosion resistance of the coating.

EIS study has also supported the potentiodynamic polarization analysis of coating's corrosion performance in Ringer's solution. An equivalent two-layer model circuit is

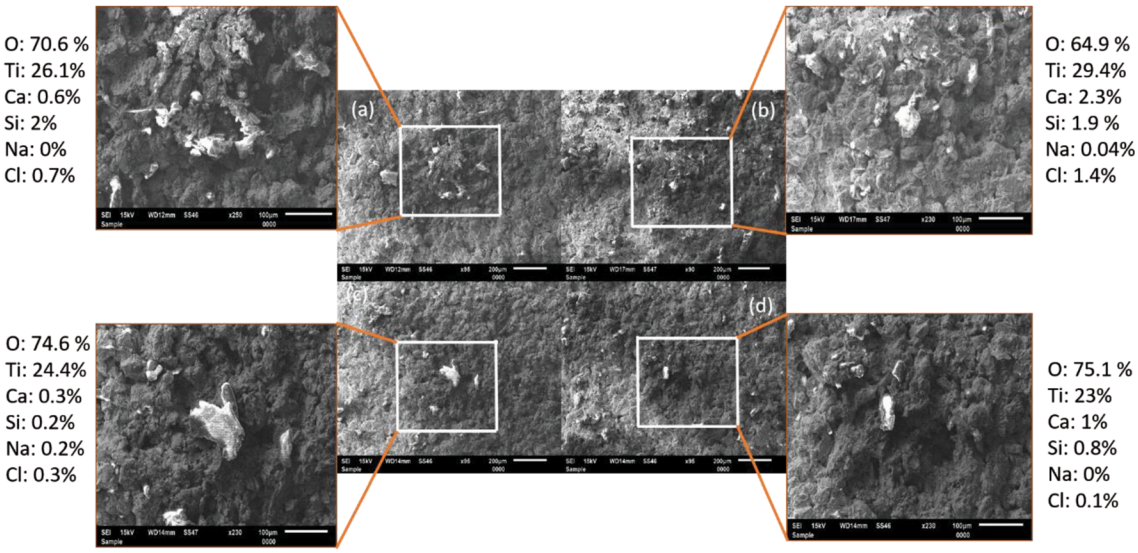

Fig. 12 Surface SEM micrograph of corroded cold sprayed Ti/BAG composite coatings after immersion in Ringer's solution for 40 h (a) Ti/10BAG (b) Ti/15BAG (c) Ti/20BAG (d) Ti/25BAG

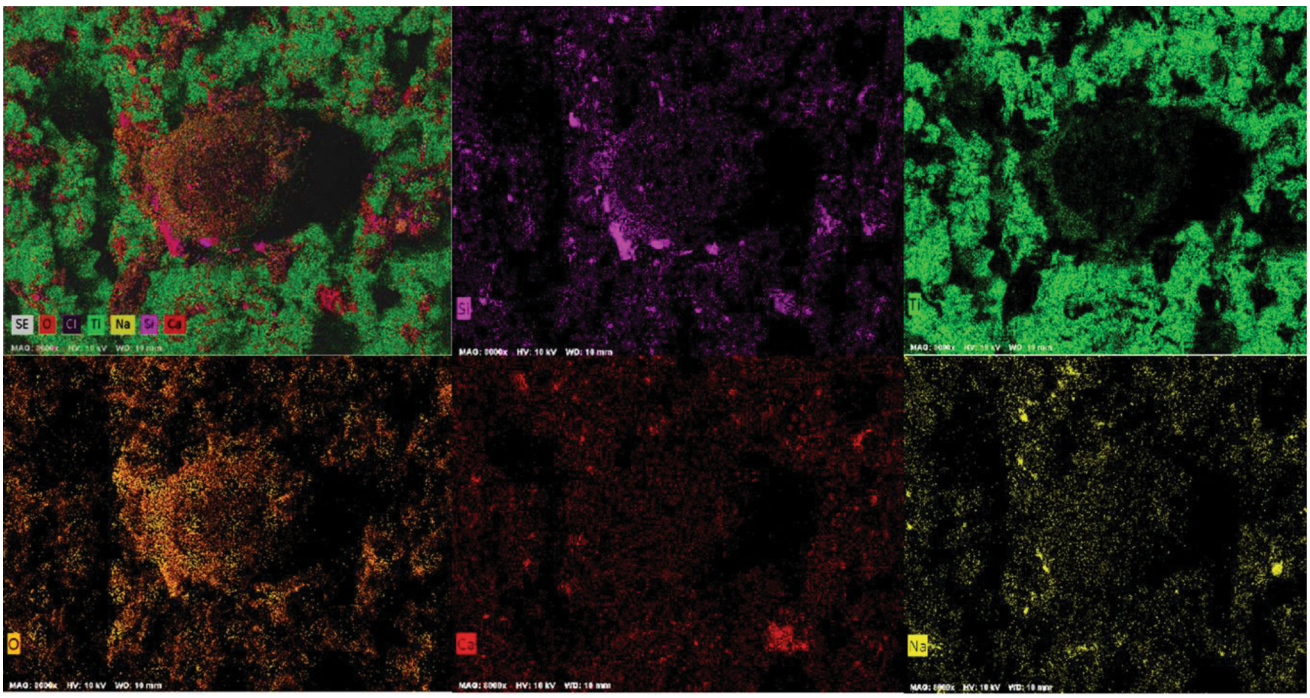

Fig. 13 Surface EDS mappings of the corroded cold sprayed Ti/25BAG composite coating on SS316L after 2 h of immersion in Ringer's solution

fitted to calculate the physical parameters of the corrosion behavior, as shown in Fig. 16. R_s in the equivalent circuit represents the electrolytic resistance, R_p as the charge transfer resistance of the coating, C_p as the capacitance of developed coatings, R_b as the polarization resistance of substrate, and the double layer capacitance as C_b. R_h and C_h represent the capacitance and resistance of precipitates into the pores. Figure 17 displays the Nyquist representation of impedance for Ti/BAG composite coatings. Data are plotted versus immersion time in Ringer's solution. The shape of the plot for all the coating samples is the same, but the diameter is different. The capacitive loops of all the coating samples are increasing with the increase in BAG content. The results from Fig. 17 reveal that with the increase in immersion time, the coatings displayed better corrosion resistance. Figure 17(a) and

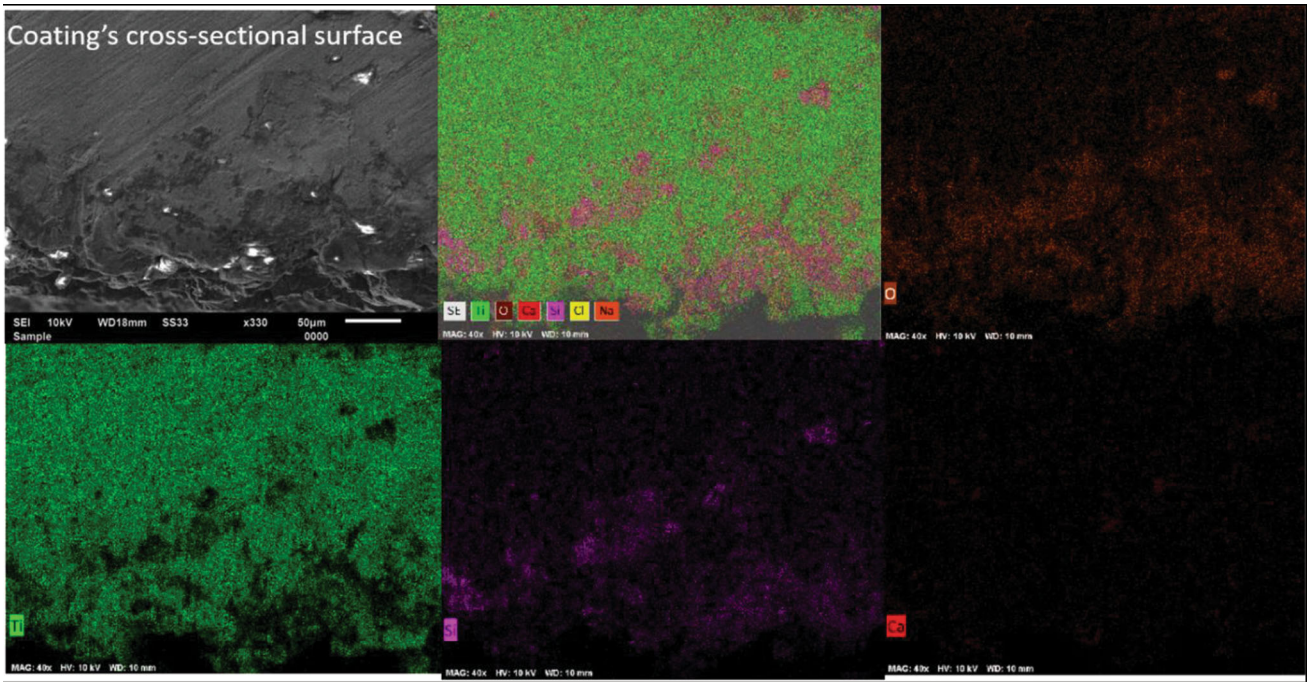

Fig. 14 Cross-sectional SEM micrograph and EDS mappings of corroded cold sprayed Ti/25BAG composite coating on SS316L after 2 h of immersion in Ringer's solution

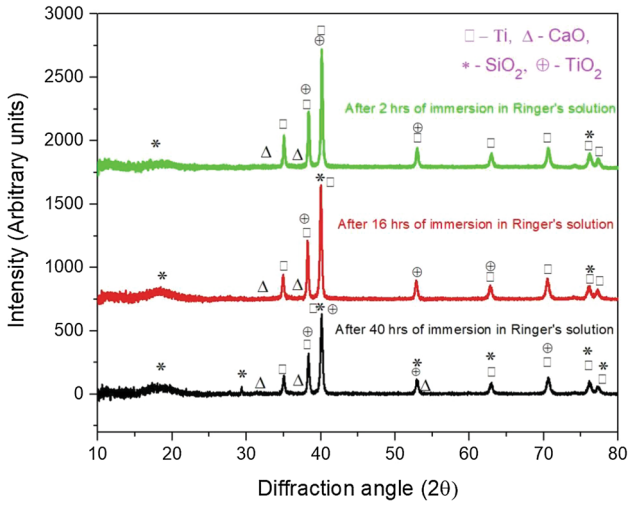

Fig. 15 XRD analysis of corroded cold sprayed Ti/25BAG composite coating on SS316L with 2 h, 16 h, and 40 h of immersion time in Ringer's solution

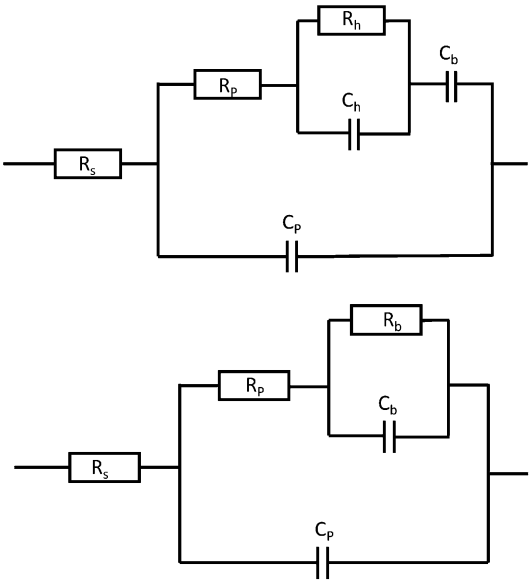

Fig. 16 Equivalent circuit fitted for EIS analysis of Ti/BAG composite coatings on SS316L

(b) shows that in the case of 2 h and 16 h of immersion after the formation of the first oxide layer, the second layer started releasing ions in each type of the coatings. However, in the case of 40 h of immersion (Fig. 17c), the only first layer is corroded. The capacitive loop in Fig. 17(d) is increasing with time which indicates that the surface becomes more stable with immersion time in Ringer's solution. The Bode plot (Fig. 18) also depicts that all the coatings are capacitive in nature. In the lower frequency region, the impedance value is consistent with the increase in BAG content and the increment in immersion time, which is a good indicator that the developed Ti/BAG composite coatings exhibit an anti-corrosion behavior. Furthermore, it was observed that even after 40 h of exposure in Ringer's solution, the coatings were well intact with the substrate. There was no evidence observed from potentiodynamic or EIS results that indicates the removal

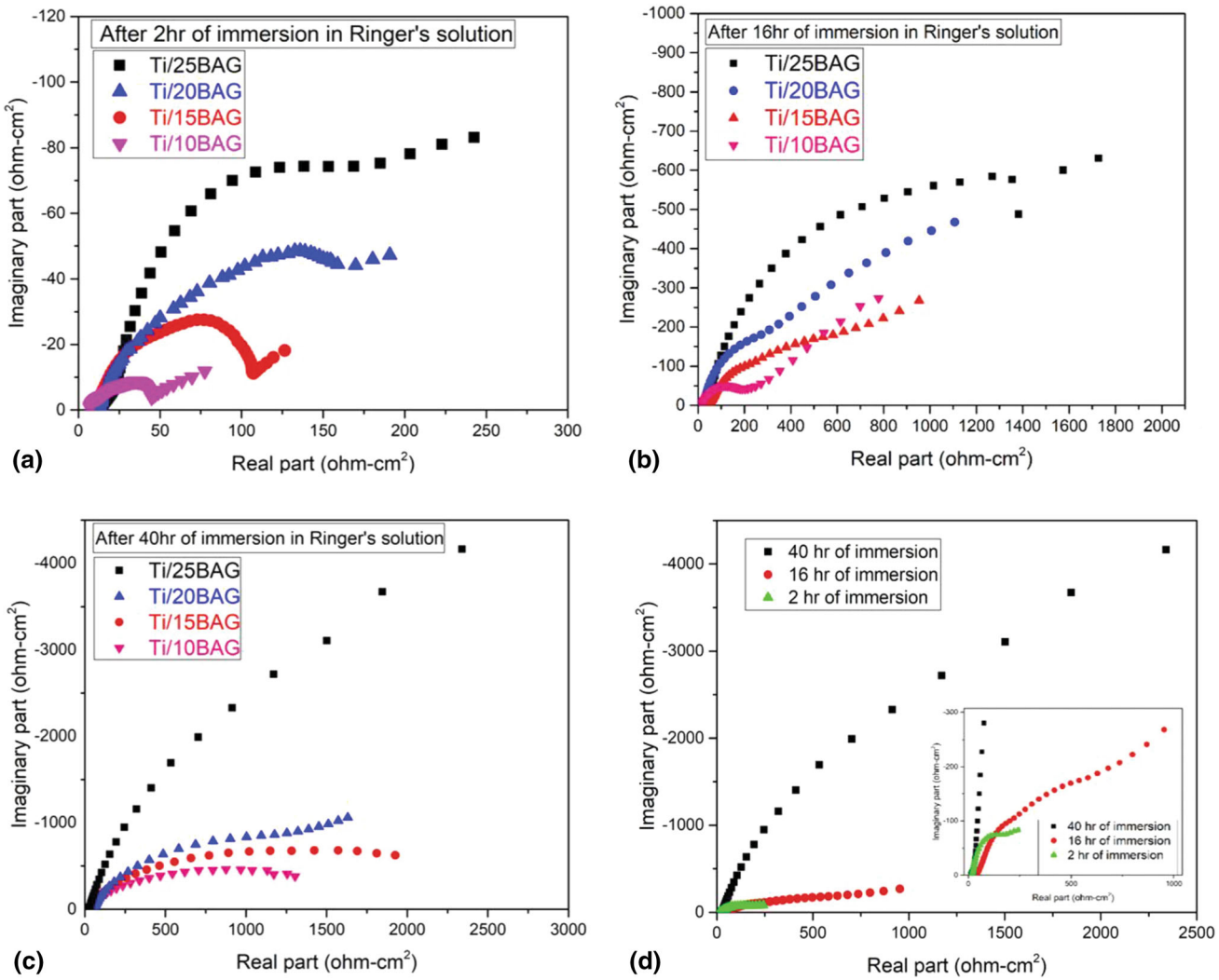

Fig. 17 Nyquist behavior of cold sprayed Ti/BAG composite coatings on SS316L in Ringer's solution (a) 2 h of immersion time (b) 16 h of immersion time (c) 40 h of immersion time (d) Ti/25BAG with immersion time

of coating from the substrate. Hence, the composite coatings are more resistant to corrosion relative to the bare substrate.

The corrosion rate (Table 4) for each of the investigated coatings is found to be below 1 micron/year. As per the ISO standard (Ref 54), if the corrosion rate is less than 1 micron/year, the surface would be considered perfectly stable. Zhou and Mohanty (Ref 55) developed cold sprayed pure Ti and 20 wt.% HA/Ti composite coating and reported E_{corr} and I_{corr} values for Ti as- 0.362 μA/cm^2 and − 241.9 mV and for 20 wt.% HA/Ti as 0.934 μA/cm^2 and − 379.9 mV in a simulated body fluid. Compared with them, the Ti/20BAG cold sprayed composite coating shows better E_{corr} and I_{corr} values (0.668 μA/cm^2 and -178.3 mV). It indicates that the cold sprayed Ti/20BAG composite coating outperformed the cold sprayed pure Ti and 20 wt.% HA/Ti composite coating in simulated body fluid environment. Furthermore, results reveal that Ti/25BAG composite coating performed even better compared to Ti/20BAG composite coating in simulated body fluid environment.

In the developed cold sprayed composite coatings, usually, porosity was available on the sites of ceramic (BAG) particles as ceramics do not bond with metal/ceramic and results in porosity, which increases with the increment of ceramic retention. The corrosion performance of these coatings has improved with the increment in porosity. The possible reason can be the formation of passive oxides such as TiO_2, SiO_2, and CaO in simulated body fluid owing to the dissolution of BAG, as shown in Fig. 15. Also, the formation of these oxides may have increased with the increment in BAG content, leading to a better corrosion resistance. In other words, BAG may have

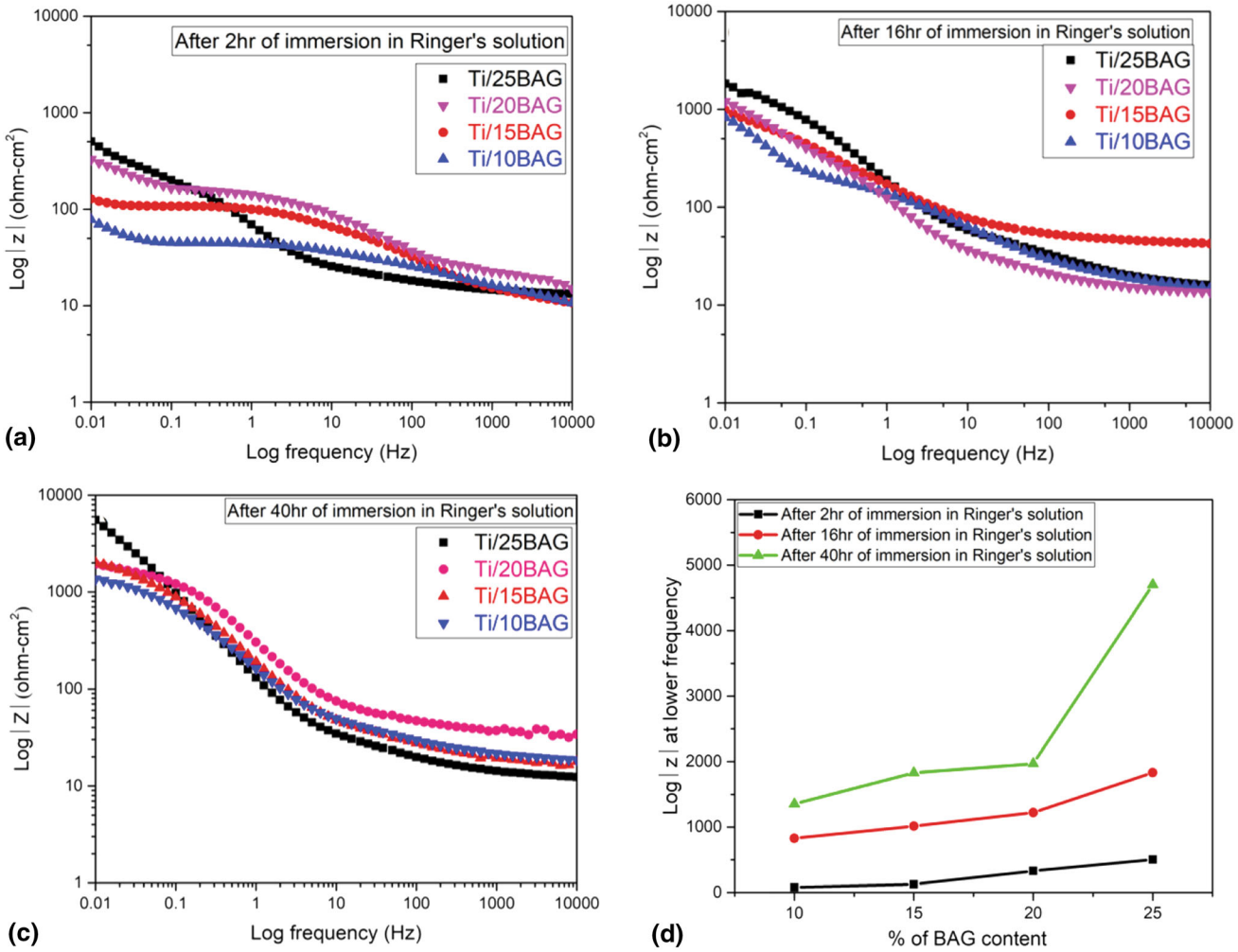

Fig. 18 Bode plot of the cold sprayed Ti/BAG composite coatings on SS316L (a) 2 h of immersion (b) 16 h of immersion (c) 40 h of immersion, and (d) impedance at low frequency (Log 0.01, Hz)

compensated for the effect of available porosity. In this context, Fojt et al. (Ref 56) have reported that materials having more than 15% porosity may lead to the localized corrosion effect, whereas corrosion performance of less porous surfaces (<15%) might be comparable with bulk surfaces. Sometimes, porosity may enhance corrosion resistance by blocking the pores due to the precipitation of Ringer's salt (Ref 57, 58).

Cell Viability

The percentage of cell viability after 24 h of incubation with change in BAG percentage is shown in Fig. 19. The percentage of cell viability for all the samples was above the threshold limit, that is, 70%, which indicates that the developed cold sprayed coatings were biocompatible and had no cytotoxic effects. The percentage of cell viability has increased with the increment in BAG content. It is well established that Ti is biocompatible but not bioactive (Ref 59). However, BAG is well accepted as a biocompatible, bioactive, and osteoconductive material (Ref 18, 60). Moreover, the other possible reasons behind the increment in cell viability of Ti/BAG composite coatings can be the increment in surface roughness and porosity caused by the addition of BAG (Fig. 7).

Conclusions

The high-pressure cold spray technology was used for the successful deposition of Ti/BAG composite coatings on SS316L for bio-implant applications. Four different compositions were synthesized and analyzed for the corrosion

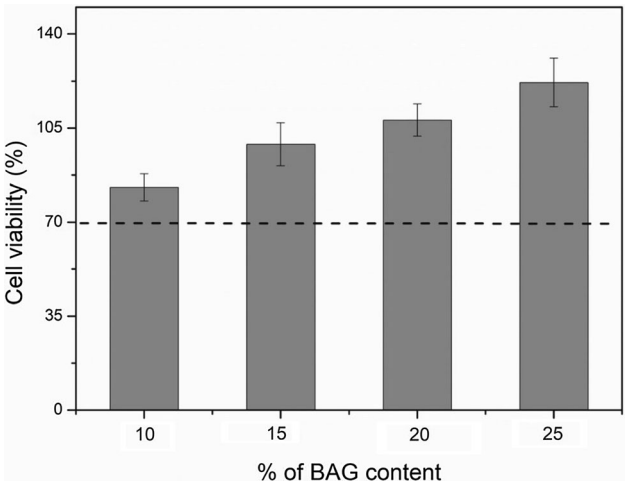

Fig. 19 Mouse preosteoblast (MC3T3-E1) cell behavior on cold sprayed Ti/BAG composite coatings over SS316L steel

behavior in simulated body fluid. Based upon the results, the following conclusions are drawn:

- The as-sprayed coatings are found to be intact with the substrate steel with a composite like structure having Ti as the matrix embedded with BAG. Moreover, there are no cracks on the surface of the produced coatings.
- The surface roughness and porosity of the developed coatings are found to be increased with the increase in BAG content.
- Potentiodynamic scans display that the corrosion resistance of SS316L improved significantly after the application of cold sprayed composite coating of Ti/BAG. This could be attributed to the formation of protective oxides such as TiO_2, SiO_2, and CaO in the corroded scales of the coatings.
- The potentiodynamic polarization curves indicate that the corrosion resistance of the composite coatings increases with the increase in BAG content.
- EIS results depict the two-layer (thin inner layer and outer porous layer) model of the oxide film for 2 h and 16 h of immersion time. The results confirm that corrosion resistance increases with the progression in BAG content.
- Based on the analysis, Ti/25BAG cold sprayed coating could be recommended as the potential coating for the given steel which even outperformed Ti/HA composite coating.

Acknowledgments The cold spray system used for this study was established through MHRD-DST funded Uchhatar Avishkar Yojana (UAY, IITRPR_001). The feedstock material used in this study was provided by Dr. Andrew Ang (Swinburne University of Technology, Melbourne Australia). The authors would also like to thank the Department of Science and Technology (DST-FIST, SR/FST/ETI-379/2014) India for the financial support, which helped in accessing the SEM and EDS facility to carry out this work. These supports are gratefully acknowledged.

Conflict of interest The authors declare that the work described in this paper has neither been published previously nor is under consideration for publication elsewhere. The contents of the paper are approved by all the authors and tacitly or explicitly by the reasonable authorities where the work was carried out. If accepted, the content of this paper will not be published elsewhere in the same form in English or in any other language, including electronically without the written consent of the copyright holder.

References

1. E. Qvistgaard, R. Christensen, S. Torp-Pedersen and H. Bliddal, Intra-articular Treatment of Hip Osteoarthritis: A Randomized Trial of Hyaluronic Acid, Corticosteroid, and Isotonic Saline, *Osteoarthr. Cartil.*, 2006, **14**, p 163–170. https://doi.org/10.1016/j.joca.2005.09.007
2. S.J.L. Sullivan and L.D.T. Topoleski, Surface Modifications for Improved Wear Performance in Artificial Joints: A Review, *JOM*, 2015, **67**, p 2502–2517. https://doi.org/10.1007/s11837-015-1543-0
3. N. Eliaz, Corrosion of Metallic Biomaterials: A Review, *Materials (Basel).*, 2019 https://doi.org/10.3390/ma12030407
4. B.N. Popov, *Corrosion Engineering: Principles and Solved Problems*, Elsevier, Amsterdam, 2015. https://doi.org/10.1016/C2012-0-03070-0
5. T. Gluck, Die Invaginationsmethode der Osteo- und Arthroplastik, *Berliner Klin. Wochenschrift.*, 1890, **44**, p 752–757.
6. B. Dikici and M. Topuz, Production of Annealed Cold-Sprayed 316L Stainless Steel Coatings for Biomedical Applications and Their in-vitro Corrosion Response, *Prot. Met. Phys. Chem. Surf.*, 2018, **54**, p 333–339. https://doi.org/10.1134/S2070205118020168
7. I. Papageorgiou, C. Brown, R. Schins, S. Singh, R. Newson, S. Davis, J. Fisher, E. Ingham and C.P. Case, The Effect of Nano- and Micron-Sized Particles of Cobalt-Chromium Alloy on Human Fibroblasts in vitro, *Biomaterials*, 2007, **28**, p 2946–2958. https://doi.org/10.1016/j.biomaterials.2007.02.034
8. J. Sharan, S.V. Lale, V. Koul, M. Mishra and O.P. Kharbanda, An Overview of Surface Modifications of Titanium and Its Alloys for Biomedical Applications, *Trends Biomater. Artif. Organs.*, 2015, **29**, p 176–187.
9. M. Kaur and K. Singh, Review on Titanium and Titanium Based Alloys as Biomaterials for Orthopaedic Applications, *Mater. Sci. Eng. C.*, 2019, **102**, p 844–862. https://doi.org/10.1016/j.msec.2019.04.064
10. Q. Chen and G.A. Thouas, Metallic Implant Biomaterials, *Mater. Sci. Eng. R Rep.*, 2015, **87**, p 1–57. https://doi.org/10.1016/j.mser.2014.10.001
11. J. Pouilleau, D. Devilliers, F. Garrido, S. Durand-Vidal and E. Mahé, Structure and Composition of Passive Titanium Oxide Films, *Mater. Sci. Eng. B.*, 1997, **47**, p 235–243. https://doi.org/10.1016/S0921-5107(97)00043-3
12. H.I. Mohammed, W.I. Abdel-Fattah, M.A. Sallam, M.E. El-Sayed, M.S.E.H. Talaat, J. Faerber, G. Pourroy, T. Roland and A. Carradò, Calcium Phosphate Coating on Ti6Al4V by Autocatalytic Route, Bioinspired, *Biomim. Nanobiomaterials.*, 2012, **1**, p 221–228. https://doi.org/10.1680/bbn.12.00012
13. S.R. Paital and N.B. Dahotre, Calcium Phosphate Coatings for Bio-implant Applications: Materials, Performance Factors, and Methodologies, *Mater. Sci. Eng. R Rep.*, 2009, **66**, p 1–70. https://doi.org/10.1016/j.mser.2009.05.001

14. V. Chalisgaonkar, M. Das and V.K. Balla, Laser Processing of Ti Composite Coatings Reinforced with Hydroxyapatite and Bioglass, *Addit. Manuf.*, 2018, **20**, p 134–143. https://doi.org/10.1016/j.addma.2018.01.008
15. H. Anawati, H. Tanigawa, T. Asoh, M. Ohno and S. Kubota, Ono, Electrochemical Corrosion and Bioactivity of Titanium-Hydroxyapatite Composites Prepared by Spark Plasma Sintering, *Corros. Sci.*, 2013, **70**, p 212–220. https://doi.org/10.1016/j.corsci.2013.01.032
16. J.J. Li, A. Akey, C.R. Dunstan, M. Vielreicher, O. Friedrich, D.C. Bell and H. Zreiqat, Effects of Material-Tissue Interactions on Bone Regeneration Outcomes Using Baghdadite Implants in a Large Animal Model, *Adv. Healthc. Mater.*, 2018, **7**, p 1–9. https://doi.org/10.1002/adhm.201800218
17. V. Abbasian, R. Emadi and M. Kharaziha, Biomimetic Nylon 6-Baghdadite Nanocomposite Scaffold for Bone Tissue Engineering, *Mater. Sci. Eng. C.*, 2020, **109**, 110549. https://doi.org/10.1016/j.msec.2019.110549
18. D.Q. Pham, C.C. Berndt, U. Gbureck, H. Zreiqat, V.K. Truong and A.S.M. Ang, Mechanical and Chemical Properties of Baghdadite Coatings Manufactured by Atmospheric Plasma Spraying, *Surf. Coatings Technol.*, 2019, **378**, 124945. https://doi.org/10.1016/j.surfcoat.2019.124945
19. Z. Gou and J. Chang, Synthesis and in vitro Bioactivity of Dicalcium Silicate Powders, *J. Eur. Ceram. Soc.*, 2004, **24**, p 93–99. https://doi.org/10.1016/S0955-2219(03)00320-0
20. Y. Liang, Y. Xie, H. Ji, L. Huang and X. Zheng, Excellent Stability of Plasma-Sprayed Bioactive $Ca_3ZrSi_2O_9$ Ceramic Coating on Ti-6Al-4V, *Appl. Surf. Sci.*, 2010, **256**, p 4677–4681. https://doi.org/10.1016/j.apsusc.2010.02.071
21. Y. Ramaswamy, C. Wu, A. Van Hummel, V. Combes, G. Grau and H. Zreiqat, The Responses of Osteoblasts, Osteoclasts and Endothelial Cells to Zirconium Modified Calcium-Silicate-Based Ceramic, *Biomaterials*, 2008, **29**, p 4392–4402. https://doi.org/10.1016/j.biomaterials.2008.08.006
22. A. Najafinezhad, M. Abdellahi, H. Ghayour, A. Soheily, A. Chami and A. Khandan, A Comparative Study on the Synthesis Mechanism, Bioactivity and Mechanical Properties of Three Silicate Bioceramics, *Mater. Sci. Eng. C.*, 2017, **72**, p 259–267. https://doi.org/10.1016/j.msec.2016.11.084
23. M.Z. Ibrahim, A.A.D. Sarhan, F. Yusuf and M. Hamdi, Biomedical Materials and Techniques to Improve the Tribological, Mechanical and Biomedical Properties of Orthopedic Implants: A Review Article, *J. Alloys Compd.*, 2017, **714**, p 636–667. https://doi.org/10.1016/j.jallcom.2017.04.231
24. A.S. Kang, G. Singh and V. Chawla, Some Problems Associated with Thermal Sprayed Ha Coatings: A Review, *Int. J. Surf. Eng. Mater. Technol.*, 2013, **3**, p 10–14.
25. R. Ghelichi and M. Guagliano, Coating by the Cold Spray Process: A State of the Art, *Frat. Ed Integrità Strutt.*, 2009, **3**, p 30–44. https://doi.org/10.3221/igf-esis.08.03
26. M.F. Smith, Comparing Cold Spray with Thermal Spray Coating Technologies, Cold Spray Mater, *Depos. Process Fundam. Appl.*, 1911, **2007**, p 43–61. https://doi.org/10.1533/9781845693787.1.43
27. A. Interanational, Standard Guide for Preparation of Metallographic Specimens Standard Guide for Preparation of Metallographic Specimens 1, *ASTM Int.*, 2012, **03**(01), p 1–12. https://doi.org/10.1520/E0003-11R17.1
28. ASTM International, Standard Test Methods for Density of Compacted or Sintered Powder Metallurgy (PM) Products Using Archimedes' Principle, Astm B962-13. p 1-7, 2013, https://doi.org/10.1520/B0962-15.2.
29. N. Chauhan and Y. Singh, L-Histidine Controls the Hydroxyapatite Mineralization with Plate-Like Morphology: Effect of Concentration and Media, *Mater. Sci. Eng. C.*, 2021, **120**, 111669. https://doi.org/10.1016/j.msec.2020.111669
30. B. Jodoin, L. Ajdelsztajn, E. Sansoucy, A. Zúñiga, P. Richer and E.J. Lavernia, Effect of Particle Size, Morphology, and Hardness on Cold Gas Dynamic Sprayed Aluminum Alloy Coatings, *Surf. Coatings Technol.*, 2006, **201**, p 3422–3429. https://doi.org/10.1016/j.surfcoat.2006.07.232
31. D. MacDonald, R. Fernández, F. Delloro and B. Jodoin, Cold Spraying of Armstrong Process Titanium Powder for Additive Manufacturing, *J. Therm. Spray Technol.*, 2017, **26**, p 598–609. https://doi.org/10.1007/s11666-016-0489-2
32. V.N.V. Munagala, V. Akinyi, P. Vo and R.R. Chromik, Influence of Powder Morphology and Microstructure on the Cold Spray and Mechanical Properties of Ti6Al4V Coatings, *J. Therm. Spray Technol.*, 2018, **27**, p 827–842.
33. T. Hussain, D.G. McCartney, P.H. Shipway and D. Zhang, Bonding Mechanisms in Cold Spraying: The Contributions of Metallurgical and Mechanical Components, *J. Therm. Spray Technol.*, 2009, **18**, p 364–379. https://doi.org/10.1007/s11666-009-9298-1
34. S. Singh, H. Singh and R.K. Buddu, Microstructural Investigations on Bonding Mechanisms of Cold-Sprayed Copper with SS316L Steel, *Surf. Eng.*, 2020, **36**, p 1067–1080. https://doi.org/10.1080/02670844.2019.1698163
35. J. Qin, Q. Huang, X. Wang, X. Suo, J. Wang and H. Li, Interfacial Metal/Ceramic Bonding Mechanism for Metallization of Ceramics via Cold Spraying, *J. Mater. Process. Technol.*, 2021, **288**, 116845. https://doi.org/10.1016/j.jmatprotec.2020.116845
36. M. Yandouzi, P. Richer and B. Jodoin, SiC Particulate Reinforced Al-12Si Alloy Composite Coatings Produced by the Pulsed Gas Dynamic Spray Process: Microstructure and Properties, *Surf. Coatings Technol.*, 2009, **203**, p 3260–3270.
37. Q. Wang, K. Spencer, N. Birbilis and M.X. Zhang, The Influence of Ceramic Particles on Bond Strength of Cold Spray Composite Coatings on AZ91 Alloy Substrate, *Surf. Coatings Technol.*, 2010, **205**, p 50–56. https://doi.org/10.1016/j.surfcoat.2010.06.008
38. E. Irissou, J.G. Legoux, B. Arsenault and C. Moreau, Investigation of Al-Al_2O_3 Cold Spray Coating Formation and Properties, *J. Therm. Spray Technol.*, 2007, **16**, p 661–668. https://doi.org/10.1007/s11666-007-9086-8
39. B.C. Sousa, M.A. Gleason, B. Haddad, V.K. Champagne, A.T. Nardi and D.L. Cote, Nanomechanical Characterization for Cold Spray: From Feedstock to Consolidated Material Properties, *Metals (Basel).*, 2020, **10**, p 1–71. https://doi.org/10.3390/met10091195
40. D. Seo, M. Sayar and K. Ogawa, SiO_2 and $MoSi_2$ Formation on Inconel 625 Surface via SiC Coating Deposited by Cold Spray, *Surf. Coatings Technol.*, 2012, **206**, p 2851–2858. https://doi.org/10.1016/j.surfcoat.2011.12.010
41. J.M. Shockley, S. Descartes, P. Vo, E. Irissou and R.R. Chromik, The Influence of Al_2O_3 Particle Morphology on the Coating Formation and Dry Sliding Wear Behavior of Cold Sprayed Al-Al_2O_3 Composites, *Surf. Coatings Technol.*, 2015, **270**, p 324–333. https://doi.org/10.1016/j.surfcoat.2015.01.057
42. An Open-Porous Titanium Coating for Advanced Osseointegration Poster No . 2216. *55th Annual Meeting of the Orthopaedic Research Society*, Vol 17, 2000, p 2216
43. N.G. Krishna, R.P. George and J. Philip, Anomalous Enhancement of Corrosion Resistance and Antibacterial Property of Commercially Pure Titanium (CP-Ti) with Nanoscale Rutile Titania Film, *Corros. Sci.*, 2020, **172**, 108678. https://doi.org/10.1016/j.corsci.2020.108678
44. C.J. Li and W.Y. Li, Deposition Characteristics of Titanium Coating in Cold Spraying, *Surf. Coatings Technol.*, 2003, **167**, p 278–283. https://doi.org/10.1016/S0257-8972(02)00919-2

45. A. Sabard, P. McNutt, H. Begg and T. Hussain, Cold Spray Deposition of Solution Heat Treated, Artificially Aged and Naturally Aged Al 7075 Powder, *Surf. Coatings Technol.*, 2020, **385**, 125367. https://doi.org/10.1016/j.surfcoat.2020.125367
46. X. Qiu, N.U.H. Tariq, L. Qi, J.Q. Wang and T.Y. Xiong, A Hybrid Approach to Improve Microstructure and Mechanical Properties of Cold Spray Additively Manufactured A380 Aluminum Composites, *Mater. Sci. Eng. A.*, 2020 https://doi.org/10.1016/j.msea.2019.138828
47. X. Qiu, N.U.H. Tariq, J. Qiang Wang, J. Rong Tang, L. Gyansah, Z. Po Zhao and T. Ying Xiong, Microstructure, Microhardness and Tribological Behavior of Al_2O_3 Reinforced A380 Aluminum Alloy Composite Coatings Prepared by Cold Spray Technique, *Surf. Coatings Technol.*, 2018, **350**, p 391–400. https://doi.org/10.1016/j.surfcoat.2018.07.039
48. D. Landolt, *Corrosion and Surface Chemistry of Metals*, CRC Press, London, 2007.
49. K.G. Neoh, X. Hu, D. Zheng and E.T. Kang, Balancing Osteoblast Functions and Bacterial Adhesion on Functionalized Titanium Surfaces, *Biomaterials*, 2012, **33**, p 2813–2822.
50. F. Qin, L. Jiang, P. Long, S. Xu, Y. Ling, Y. Yu and G. Wei, Effect of Deposition Potential on Preparation and Corrosion Resistance of SiO_2 Film on Copper, *Int. J. Electrochem. Sci.*, 2020, **15**, p 6478–6487. https://doi.org/10.20964/2020.07.49
51. M. Catauro, A. Dell'Era and S.V. Ciprioti, Synthesis, Structural, Spectroscopic and Thermoanalytical Study of Sol–Gel Derived SiO_2-CaO-P_2O_5 Gel and Ceramic Materials, *Thermochim. Acta.*, 2016, **625**, p 20–27.
52. M. Catauro, F. Barrino, M. Bononi, E. Colombini, R. Giovanardi, P. Veronesi and E. Tranquillo, Coating of Titanium Substrates with ZrO_2 and ZrO_2-SiO_2 Composites by Sol-Gel Synthesis for Biomedical Applications: Structural Characterization, Mechanical Aad Corrosive Behavior, *Coatings*, 2019 https://doi.org/10.3390/coatings9030200
53. D. Krupa, J. Baszkiewicz, B. Rajchel, A. Barcz, J.W. Sobczak and A. Biliński, Effect of Sodium-Ion Implantation on the Corrosion Resistance and Bioactivity of Titanium, *Vacuum*, 2005, **78**, p 161–166. https://doi.org/10.1016/j.vacuum.2005.01.020
54. S. ISO, 8044: 2000, *Corros. Met. Alloy. Terms Defin*. (n.d.).
55. X. Zhou and P. Mohanty, Electrochemical Behavior of Cold Sprayed Hydroxyapatite/Titanium Composite in Hanks' Solution, *Electrochim. Acta.*, 2012, **65**, p 134–140. https://doi.org/10.1016/j.electacta.2012.01.018
56. J. Fojt, L. Joska and J. Málek, Corrosion Behaviour of Porous Ti-39Nb Alloy for Biomedical Applications, *Corros. Sci.*, 2013, **71**, p 78–83. https://doi.org/10.1016/j.corsci.2013.03.007
57. J. Pan, D. Thierry and C. Leygraf, Electrochemical Impedance Spectroscopy Study of the Passive Oxide Film on Titanium for Implant Application, *Electrochim. Acta.*, 1996, **41**, p 1143–1153. https://doi.org/10.1016/0013-4686(95)00465-3
58. R.M. Souto, M.M. Laz and R.L. Reis, Degradation Characteristics of Hydroxyapatite Coatings on Orthopaedic TiAlV in Simulated Physiological Media Investigated by Electrochemical Impedance Spectroscopy, *Biomaterials*, 2003, **24**, p 4213–4221. https://doi.org/10.1016/S0142-9612(03)00362-4
59. Y. Li, S. Zou, D. Wang, G. Feng, C. Bao and J. Hu, The Effect of Hydrofluoric Acid Treatment on Titanium Implant Osseointegration in Ovariectomized Rats, *Biomaterials*, 2010, **31**, p 3266–3273. https://doi.org/10.1016/j.biomaterials.2010.01.028
60. T.C. Schumacher, E. Volkmann, R. Yilmaz, A. Wolf, L. Treccani and K. Rezwan, Mechanical Evaluation of Calcium-Zirconium-Silicate (Baghdadite) Obtained by a Direct Solid-State Synthesis Route, *J. Mech. Behav. Biomed. Mater.*, 2014, **34**, p 294–301. https://doi.org/10.1016/j.jmbbm.2014.02.021